ACS APPLIED MATERIALS & INTERFACES

www.acsami.org

Research Article

A Double Hemin Bonded G-Quadruplex Embedded in Metal−Organic Frameworks for Biomimetic Cascade Reaction

Xuanxiang Mao, Dehui Qiu, Shijiong Wei, Xiaobo Zhang, Jianping Lei, Jean-Louis Mergny, Huangxian Ju, and Jun Zhou*

Cite This: *ACS Appl. Mater. Interfaces* 2022, 14, 54598−54606

Read Online

ACCESS | Metrics & More | Article Recommendations | Supporting Information

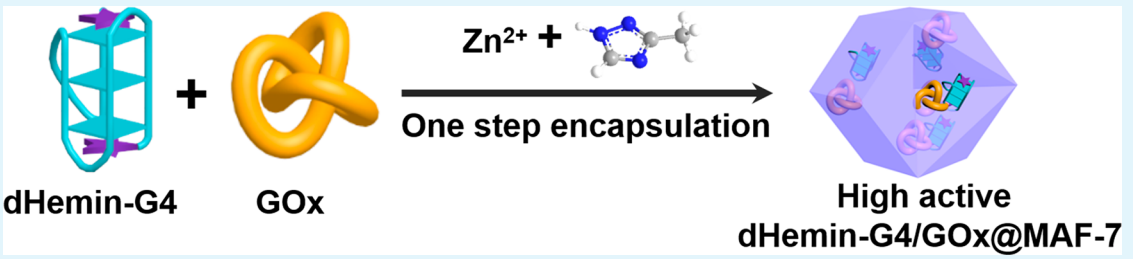

ABSTRACT: Biocatalytic transformations in living cells, such as enzymatic cascades, function effectively in spatially confined microenvironments. However, mimicking enzyme catalytic cascade processes is challenging. Herein, we report a new dual-Hemin-G-quadruplex (dHemin-G4) DNAzyme with high catalytic activity over noncovalent G4/Hemin and monocovalent counterparts (G4-Hemin and Hemin-G4) by covalently linking hemin to both ends of an intramolecular G4. We use MAF-7, a hydrophilic metal−organic framework (MOF), as the protecting scaffold to integrate a biocatalytic cascade consisting of dHemin-G4 DNAzyme and glucose oxidase (GOx), by a simple and mild method with a single-step encapsulation of both enzymes. Such a MAF-7-confined cascade system shows superior activity over not only traditional G4/Hemin but also other MOFs (ZIF-8 and ZIF-90), which was mainly attributed to high-payload enzyme packaging. Notably, the introduction of hydrophilic G4 allows to avoid the accumulation of hydrophobic hemin on the surface of MAF-7, which decreases cascade biocatalytic activity. Furthermore, MAF-7 as protective coatings endowed the enzyme with excellent recyclability and good operational stability in harsh environments, including elevated temperature, urea, protease, and organic solvents, extending its practical application in biocatalysis. In addition, the incorporated enzymes can be replaced on demand to broaden the scope of catalytic substrates. Taking advantages of these features, the feasibility of dHemin-G4/GOx@MAF-7 systems for biosensing was demonstrated. This study is conducive to devise efficient and stable enzyme catalytic cascades to facilitate applications in biosensing and industrial processes.

KEYWORDS: *G-quadruplex, hemin, G-quadruplex/hemin DNAzyme, cascade biomimetic strategy, metal−organic frameworks*

INTRODUCTION

Cascade biocatalysis, an important class of chemical transformation, is significant for biological signal transduction and metabolic pathways by providing sequential intercommunication and instant signal feedback in cellular environments.[1−5] Unsurprisingly, mimicking enzyme biocatalytic cascades for the construction of complex chemical transformation networks is receiving increasing concerns.[1,6−9] Among them, glucose oxidase (GOx) and horseradish peroxidase (HRP) constitute a typical cascade reaction system, which has been widely used in bioanalysis.[10−14] Recent efforts have been devoted to developing economical and robust HRP substitutes, such as nanozymes and DNAzymes.[15−17] Interestingly, hemin is an inexpensive and promising substitute of HRP, usually obtained from the active center of hemin-containing enzymes.[15,18] Unfortunately, hemin is a hydrophobic small molecule and shows low catalytic activity in aqueous media owing to its poor aqueous solubility and molecular aggregation.[18] To increase the catalytic activity and aqueous stability of hemin, several strategies have been proposed by modification of nanomaterials (i.e., graphene and MOFs) and anchoring to the biological macromolecules (i.e., protein, polypeptide, and G-quadruplex).[19−24]

G-quadruplexes (G4s) are unusual nucleic acid structures composed of several stacked G-quartets. G4 can be combined with hemin to form a catalytical G4/hemin DNAzyme, mimicking horseradish peroxidase (HRP), through $\pi-\pi$ stacking.[25−27] Compared with natural HRP, the G4/hemin DNAzyme not only is easier and cheaper to synthesize and

Received: October 13, 2022
Accepted: November 18, 2022
Published: December 2, 2022

https://doi.org/10.1021/acsami.2c18473
ACS Appl. Mater. Interfaces 2022, 14, 54598−54606

manipulate but also exhibits superior adaptability to inhospitable conditions.[28−30] Due to these advantages, G4/hemin DNAzyme is widely used in biosensing by catalyzing various substrates to obtain colorimetric, chemiluminescent, and fluorescent output signals.[31−35] Unfortunately, this system suffers from low catalytic efficiency due to the limited affinity of hemin to G4 (K_d ca. 10^{-7} M) compared with HRP,[36,37] which needs to be improved. Recently, our group reported an efficient system in which hemin covalently linked to the 3′-terminal of G4 can obviously enhance its catalytic activity and reduce the background signal, showing a clear advantage over nonconjugated G4/hemin.[22,23] Encouraged by the efficient catalytic performance of the conjugated G4-hemin system, we sought to explore higher catalytic activity than that of reported covalent G4-hemin system by covalent integration of hemin at both 3′- and 5′- ends of G4, denoted as dHemin-G4 DNAzyme, which has not been reported previously.

Notably, the low stability in hostile environments and poor reusability of using tandem enzymes restrict their practical applications. Recently, the spatial confinement of enzymes in metal−organic frameworks (MOFs) scaffolds offered a promising perspective to construct enzyme catalytic cascade systems. Different from the biocatalytic cascades in homogeneous aqueous phase, the introduction of MOFs can provide protection to the enzymes in harsh conditions, enhance activities, and improve the efficiency in recovery of the enzymes.[3,38−41] Zeolitic imidazolate frameworks (ZIFs) have been emerged as ideal scaffolds for the *in situ* immobilization of native enzymes because of mild synthetic conditions, their open channels, and abundant porosity, which provide opportunities for the contact between substrates and enzymes.[42,43] Among them, ZIF-8 has been widely used for biomimetic mineralization due to its biologically compatible synthetic conditions.[44,45] However, recent studies suggest that the enzymes embedded in hydrophobic ZIF-8 crystals may lose activity owing to conformational changes,[38,46] which calls for suitable alternatives capable of keeping the activity of the encapsulated enzymes. Significantly, MAF-7 with hydrophilic scaffolds is becoming an emerging material for the immobilization of enzyme with high encapsulation efficiency, which is beneficial for retaining catalytic activity by maintaining the natural conformation of enzymes.[6,38]

Herein, taking advantages of the dHemin-G4 with high catalytic performance and Zn-based MAF-7 MOF as the scaffold, we developed an efficient biocatalytic cascade nanoplatform. As shown in Scheme 1, both ends (3′- and 5′-terminal) of G4 modified with amino groups covalently bound to carboxylated hemin by simple carbodiimide/*N*-hydroxysuccinimide (NHS) method, which then annealed at 95 °C to obtain dHemin-G4 DNAzyme with higher catalytic activity than that of single-end (3′- or 5′-) functionalized G4 (these two conjugated complexes are denoted as G4-Hemin and Hemin-G4, respectively) and noncovalent G4/Hemin DNAzymes. After that, glucose oxidase (GOx) and dHemin-G4 DNAzyme are embedded in the hydrophilic MAF-7 frameworks (denoted as dHemin-G4/GOx@MAF-7, hereafter) *via* a mild *de novo* assembly in one step only. The developed cascade biocatalytic system incorporating covalently cross-linked G4 showed higher activity than individual hemin, likely due to the tendency of hydrophobic hemin to accumulate on the surface of MAF-7. In addition, the double-end cross-linked G4 was more active than the non-cross-linked and monocross-linked counterparts. This phenomenon suggests the covalent

Scheme 1. Schematic Illustration of the Preparation of the dHemin-G4/GOx@MAF-7 Composite with High Catalytic Activity

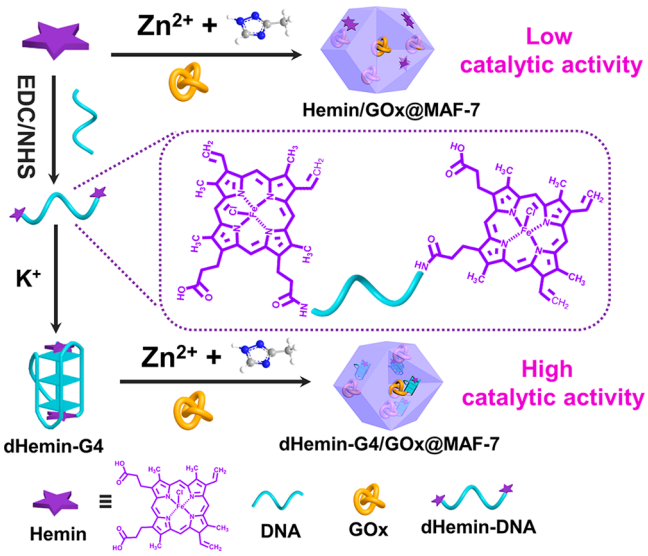

connection of G4 enhances cascade biocatalytic activity and promotes the encapsulation of hydrophobic hemin into hydrophilic MAF-7. The constructed MAF-7-confined biocatalytic cascades presented superior activity over the ZIF-8 and ZIF-90 systems, possibly because the hydrophilic microenvironment of MAF-7 increased the embedding content of enzymes. Importantly, dHemin-G4/GOx@MAF-7 exhibits good tolerance to harsh environments, including elevated temperature, urea, protease, and organic solvents, which extends its practical applicability. Additionally, the versatility of this single-step encapsulation strategy for two enzymes is also confirmed by replacing GOx with other enzymes (xanthine oxidase and urate oxidase), broadening the scope of biocatalytic substrates. These results indicate that the dHemin-G4/GOx@MAF-7 system with high stability and activity sheds light on a promising strategy of immobilizing enzymes for superior biocatalytic transformations and biosensing.

EXPERIMENTAL SECTION

Preparation of Covalent dHemin-G4. The preparation method of double hemin covalently connected to the both ends of G4 DNA sequence, 5′-CTGGGTGGGTGGGTGGGTC-3′, that is, dHemin-G4, was based on a reported method of construction of single covalent linkage of G4 and hemin with minor modifications.[22] Specifically, 1 mL of hemin DMSO solution (1 mM) was mixed with 0.5 mL of 1-(3-dimethylaminopropyl)-3-ethylcarbodiimide hydrochloride (EDC) and *N*-hydroxysuccinimide (NHS) solution (10 mM each) followed by stirring for 2 h at room temperature to activate the carboxyl group of hemin. Then, 10 μM amine-modified DNA sequences (NH_2-DNA-NH_2) dissolved in 10 mM Tris-HCl buffer (pH 7.0) were reacted with 40 μM activated NHS-hemin for another 3 h. The resulting samples were heated at 95 °C for 5 min followed by slow cooling to room temperature and stored at 4 °C overnight prior to use.

Preparation of dHemin-G4/GOx@MAF-7. $Zn(NO_3)_2{\cdot}6H_2O$ (40 mM), 120 mM 3-methyl-1,2,4-triazole, 60 μL of 10% $NH_3{\cdot}H_2O$, 5 μM dHemin-G4, and 0.5 mg mL^{-1} GOx were mixed, and ultrapure water was supplemented to make a total volume of 3 mL. The mixture was then stirred at room temperature for 24 h. The precipitate was gathered by centrifugation at 9000 rpm for 10 min and

https://doi.org/10.1021/acsami.2c18473
ACS Appl. Mater. Interfaces 2022, 14, 54598−54606

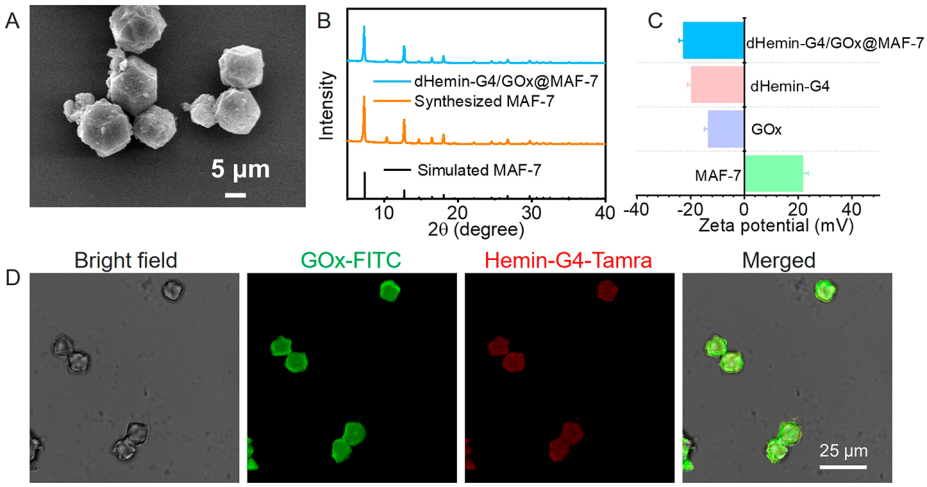

Figure 1. (A) SEM image of dHemin-G4/GOx@MAF-7. (B) Power X-ray diffraction patterns (PXRD) of simulated MAF-7, synthesized MAF-7 and dHemin-G4/GOx@MAF-7 samples. (C) ζ potentials of MAF-7, GOx, dHemin-G4, and dHemin-G4/GOx@MAF-7. (D) Confocal laser scanning micrographs showing Hemin-G4-Tamra/GOx-FITC@MAF-7 (from left to right: bright field, FITC-labeled GOx, Tamra-labeled Hemin-G4, and merged channel).

then washed with water for three times to remove loosely adsorbed dHemin-G4 and GOx.

Activity Assay of Confined Biocatalytic Cascade. The activities of these confined tandem biocatalysis were evaluated by recording the $ABTS^{\bullet+}$ at 420 nm using a UV−vis spectrophotometer. Concretely, the biocatalytic cascade assay was performed in 500 μL of Tris-HCl buffer (10 mM, pH 7.0) containing 0.5 mg of MAF-7-confined cascade nanoparticles, 200 μM ABTS, and 2 mM substrate. ZIF-8- and ZIF-90-confined cascade nanoparticles with equal enzymes embedding were used as the controls. The catalytic reaction was activated by adding the substrates (glucose, uric acid, and xanthine, respectively). The activity of the biocatalytic cascade reaction was monitored by tracing the UV spectra of the generated $ABTS^{\bullet+}$ (420 nm) for 10 min.

Stability Assay. To demonstrate the protective effect of MAF-7 on the encapsulated dHemin-G4/GOx, the equivalent amount of two samples, dHemin-G4/GOx and dHemin-G4/GOx@MAF-7, were incubated at elevated temperature or aqueous solution containing urea, trypsin, organic solvents including *N*,*N*-dimethylformamide (DMF), dimethyl sulfoxide (DMSO), and tetrahydrofuran (THF) at 37 °C for 4 h, respectively. The protective effect was estimated by the detection of enzymatic activities of the samples.

Glucose Determination. Glucose detection was performed on real human serum samples from Jiangsu Province Hospital (Nanjing, China). First, the calibration curve for glucose was developed. In detail, 0.1 mL of 0.25 mg mL^{-1} dHemin-G4/GOx@MAF-7 and 0.05 mL of glucose solution with various concentrations were mixed with 0.1 mL of 10 mM Tris-HCl buffer (pH 7.0), followed by incubating at 37 °C for 30 min. The obtained solution was added into 0.05 mL of 0.5 mM luminol and diluted to 0.5 mL with B-R buffer (pH 8.5), which were used for standard curve experiments. Second, for the analysis of glucose in real samples, human serum samples were gathered by ultrafiltration at 3600 rpm for 30 min. The collected filtrate was diluted by 100-fold. Then, 0.01 mL of the diluted filtrate and 0.1 mL of 0.25 mg mL^{-1} dHemin-G4/GOx@MAF-7 were mixed with 10 mM Tris-HCl buffer (pH 7.0). After incubating at 37 °C for 30 min, the mixture with 50 μM of luminol was diluted to 0.5 mL with water for chemiluminescence detection.

RESULTS AND DISCUSSION

Characterization of dHemin-G4/GOx@MAF-7. First, the covalent linkage between NH_2-G4-NH_2 and hemin (denoted as dHemin-G4, and the G4 DNA sequence used here is CTGGGTGGGTGGGTGGGTC) was confirmed by several physicochemical techniques. The Fourier-transform infrared (FT-IR) spectra (Figure S1) showed two typical peaks (1639 and 1562 cm^{-1}) within the spectra of dHemin-G4, which were attributed to the formation of amide bonds,[47] demonstrating the covalent linkage between G4 and hemin. Further, the mass spectrum of dHemin-G4 revealed a mass of 7612.7, in agreement with the calculated mass (7613) (Figure S2), indicating the formation of the expected structure.

Next, the obtained products were characterized by different techniques to better understand their actual structure. The crystal morphology was estimated by scanning electron microscopy (SEM) and transmission electron microscopy (TEM). Compared with the dispersed rhombododecahedral crystals of MAF-7 (Figures S3 and S4A), the dHemin-G4/GOx@MAF-7 samples were more irregular intergrowth crystals (Figure 1A and Figures S4B), demonstrating that the integration of dHemin-G4 and GOx into the MAF-7 coatings affected its morphology. Further, the PXRD spectrum (Figure 1B) of dHemin-G4/GOx@MAF-7 agrees well with those of the standard structure of simulated or synthesized MAF-7, confirming that the good crystallinity of MAF-7 was retained after the encapsulation of dHemin-G4/GOx. Then, zeta (ζ) potentials showed that GOx and dHemin-G4 were negatively charged in aqueous solution, with charges of −13.3 and −19.6 mV (Figure 1C), respectively, which can easily absorb positively charged Zn^{2+} in the precursor solution of MAF-7. Compared with the positively charged MAF-7, the ζ potential of the as-prepared dHemin-G4/GOx@MAF-7 was −22.5 mV, revealing its good solubility. As revealed by the full X-ray photoelectron spectra, compared with pristine MAF-7, the dHemin-G4/GOx@MAF-7 biocatalysts showed the coexistence of C, Zn, N, O, P, and Fe elements (Figure S5A). Further, the high-resolution XPS spectra of Zn 2p (Figure S5B) indicated that the binding energy peaks about 1021.7 and 1044.8 eV were corresponding to Zn $2p_{3/2}$ and Zn $2p_{1/2}$, respectively, which was in accordance with the reported MAF-7 MOFs.[6] Additionally, the thermal gravimetric analysis (TGA) was conducted in N_2 to confirm the encapsulation of dHemin-G4/GOx in the MAF-7 coatings (Figure S6).[38] To demonstrate the spatial distribution and the encapsulation of dHemin-G4/GOx into MAF-7, Hemin-G4-Tamra/GOx-FITC@MAF-7 was synthesized, where GOx was labeled with

https://doi.org/10.1021/acsami.2c18473
ACS Appl. Mater. Interfaces 2022, 14, 54598−54606

FITC and Hemin-G4 was labeled with Tamra for imaging on a confocal laser scanning microscope. As shown in Figure 1D, the clear green and red fluorescent polyhedrons corresponding to GOx-FITC and Hemin-G4-Tamra, respectively, were distributed evenly within the Hemin-G4-Tamra/GOx-FITC@MAF-7 crystals, confirming the integration of GOx and Hemin-G4 into MAF-7 coatings. The same sample was further analyzed by imaging from top to down through Z-stack collection and Z-projection, verifying G4 and GOx were encapsulated in MAF-7 (Figure S7).

Then, the N_2 adsorption and desorption isotherms were used to assess the surface area and porosity. As displayed in Figure 2A, the dHemin-G4/GOx@MAF-7 exhibited type-I

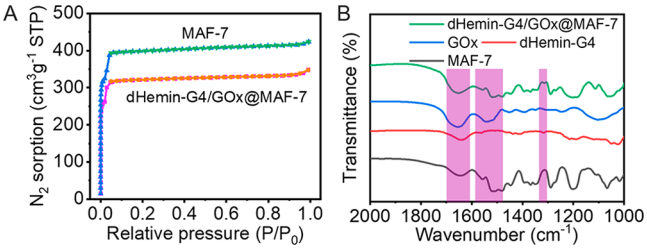

Figure 2. (A) N_2 adsorption and desorption isotherms for MAF-7 and dHemin-G4/GOx@MAF-7. (B) FT-IR spectra of MAF-7, GOx, dHemin-G4, and dHemin-G4/GOx@MAF-7 biohybrids.

isotherms with a surface area of 977.02 m^2 g^{-1}, which was lower than that of bare MAF-7 (1207.29 m^2 g^{-1}), suggesting that MAF-7 with a large specific surface area was instrumental in high dHemin-G4/GOx loading and the embedding dHemin-G4/GOx into MAF-7 would lead to the decrement of the surface area. Furthermore, the distribution of pore size was calculated to be 8.6 Å, demonstrating that the incorporation of dHemin-G4 and GOx into MAF-7 did not influence the MOF micropore structure and allowed the entrance of the substrates to interact with the embedded GOx and dHemin-G4 molecules (Figure S8). In addition, FT-IR spectra (Figure 2B) displayed the characteristic amide I (1700−1610 cm^{-1}) and amide II (1595−1480 cm^{-1}) bands corresponding to the typical peptide skeleton of GOx.[9] Furthermore, the typical bands (1562 and 1317 cm^{-1}) of dHemin-G4 were observed in dHemin-G4/GOx@MAF-7, again indicating GOx and dHemin-G4 were incorporated into MAF-7. As shown in Figure S9, the UV absorption peak of hemin in aqueous solution showed a blue-shifted and broadened peak around 371 nm, confirming the formation of the dimer of hemin. Similarly, the characteristic peak of Hemin/GOx@MAF-7 was analogous to that of hemin dimer, indicating the accumulation of hydrophobic hemin on the surface of MAF-7. For comparison, the characteristic UV absorption peak of hemin in DMSO solvent located at 404 nm, which illustrated the presence of hemin monomer.[48] The UV absorption peaks of dHemin-G4 and dHemin-G4/GOx@MAF-7 were also at 404 nm, demonstrating that the introduction of G4 prevented the accumulation of hydrophobic hemin on the surface of MAF-7. Additionally, as revealed by UV absorption peak of dHemin-G4/GOx@MAF-7, both dHemin-G4 and GOx were encapsulated in MAF-7 scaffolds. Taken together, all these results confirmed that these two enzymes were successfully encapsulated into the framework of MAF-7 as expected.

Catalytic Performance of dHemin-G4/GOx@MAF-7 toward Glucose. It is well-known that hydrophobic hemin possesses low catalytic activity in aqueous solution due to dimerization, and the introduction of G4 can form a noncovalent G4/hemin DNAzyme system with HRP-like activity.[17,18] Recently, our group reported that covalently anchored hemin at the 3-terminal of G4 was more active than the previous nonconjugated system,[22,23] which stimulated us to test whether covalent attachment of hemin to both ends of G4 (3′- and 5′-terminal, denoted as dHemin-G4) would further improve the peroxidase activity of the system. As expected, the catalytic activity of the dHemin-G4 DNAzyme system coupled with hemin at both ends of G4 was significantly higher than that of noncovalent G4/hemin and also was 182 times higher than that of hemin. More interestingly, the catalytic activity of double covalent system is higher than that of monoend cross-linked hemin (e.g., Hemin-G4 and G4-Hemin, which represented hemin linked at 5′- and 3′-end, respectively) (Figure 3A and Figure S10). The possible reasons are (i)

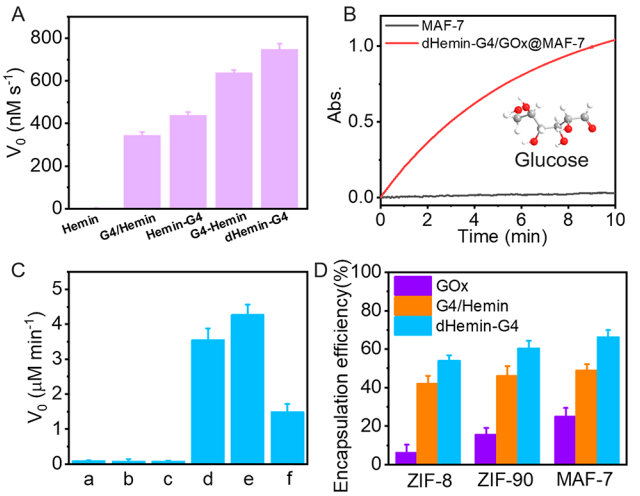

Figure 3. (A) Peroxidase activity of Hemin, nonconjugated G4/hemin, Hemin-G4 (Hemin covalently binds to 5′- end of G4 DNA), G4-Hemin (Hemin covalently binds to 3′- end of G4 DNA), and dHemin-G4 (Hemin covalently binds to both ends (5′- and 3′-ends) of G4 DNA). (B) Chemical transformation of dHemin-G4/GOx@MAF-7 with 1 mM glucose. (C) Initial velocity (V_0) of biocatalytic cascade reactions (a, ZIF-90; b, MAF-7; c, ZIF-8; d, dHemin-G4/GOx@ZIF-90; e, dHemin-G4/GOx@MAF-7; f, dHemin-G4/GOx@ZIF-8) in the presence of 1 mM glucose. (D) Encapsulation efficiency of GOx, noncovalent G4/Hemin, and covalent dHemin-G4 within different MOFs (ZIF-8, ZIF-90, and MAF-7).

proximal nucleobases in the G4 enhance the catalytic ability of the dHemin-G4 DNAzyme[23] and (ii) a better stability and more exposed active sites are obtained after coupling with hemin at both ends of G4 because free hemin tends to dimerize in aqueous solution. Thus, we chose dHemin-G4 together with glucose oxidase to construct the efficient biocatalytic cascade reaction in the framework of hydrophilic MAF-7. In this bienzyme cascade reaction, H_2O_2 was generated by the aerobic oxidation of glucose by GOx, which conducted as a substrate for dHemin-G4 with outstanding HRP-like activity and catalyzed the oxidation of classical substrates (i.e., ABTS and luminol). As the result shown in Figure 3B, the glucose (ca. 4.2 × 5.4 Å) activated cascade transformations of dHemin-G4/GOx@MAF-7, revealing glu-

https://doi.org/10.1021/acsami.2c18473
ACS Appl. Mater. Interfaces 2022, 14, 54598−54606

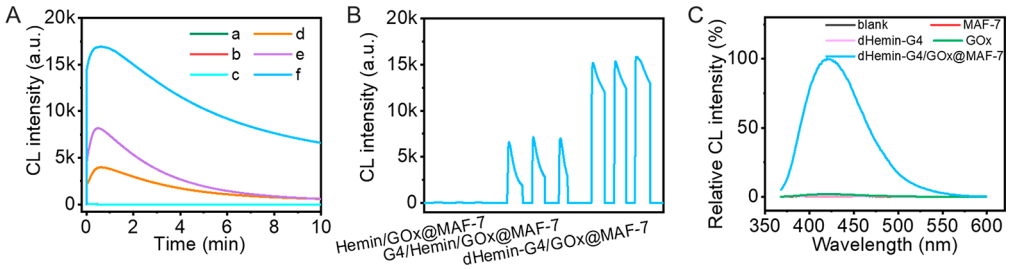

Figure 4. (A) Kinetic characteristics of the luminol-glucose CL system with different catalysts (a, ZIF-8; b, ZIF-90; c, MAF-7; d, dHemin-G4/GOx@ZIF-8; e, dHemin-G4/GOx@ZIF-90; f, dHemin-G4/GOx@MAF-7) in the presence of 1 mM glucose. Note: the spectra of a, b, and c are overlapped. (B) Catalytic activity of Hemin/GOx@MAF-7, G4/Hemin/GOx@MAF-7, and dHemin-G4/GOx@MAF-7 with 1 mM glucose. (C) CL spectra of the luminol-glucose system with different catalysts (MAF-7, dHemin-G4, GOx, and dHemin-G4/GOx@MAF-7).

cose diffused into the scaffolds of MAF-7 and interacted with the embedded dHemin-G4 and GOx molecules.

To deeply explore the biocatalytic cascade behaviors of two enzymes in MOFs, the analogous system that dHemin-G4/GOx with identical dosage was encapsulated into highly crystallized ZIF-8 and ZIF-90 MOF for comparison (Figure 3C and Figure S11). These results again demonstrated the relevance of our previous choice, as dHemin-G4/GOx@MAF-7 displayed the best biocatalytic cascade activity (with an initial velocity V_0 of 4.26 μM min^{-1}). This may be attributed to the fact that dHemin-G4 and GOx were easier to encapsulate in the hydrophilic structure of MAF-7 than in ZIF-8 and ZIF-90 (with initial velocities V_0 of 1.48 and 3.54 μM min^{-1}, respectively). To further confirm this assumption, we added the same dose of dHemin-G4 and GOx into the precursor solution of biohybrids, collected the supernatant and measured their absorbance after sufficient reaction, and calculated the encapsulation efficiency of the corresponding enzyme by the BCA method and hemin standard curve method (Figure S12). As shown in Figure 3D, MAF-7 allowed to package more dHemin-G4 and GOx (66.1% and 24.9%, respectively) than ZIF-8 (53.9% and 6.1%, respectively) and ZIF-90 (60.3% and 15.5%, respectively), demonstrating more efficient encapsulation of MAF-7 than ZIF-8 and ZIF-90. Surprisingly, compared with noncovalent G4/Hemin, the covalent combination of both ends of G4 and hemin improved the encapsulation efficiency of hemin in hydrophilic MAF-7, which also evidenced the efficient biocatalytic cascade activity of dHemin-G4/GOx@MAF-7. Further, the loading amounts of dHemin-G4 and GOx within MAF-7 were 0.85 and 1.94 mg/g, respectively, which were higher than those of ZIF-8 and ZIF-90 (Table S1), again indicating the excellent loading capacity of MAF-7 for the encapsulation of dHemin-G4 and GOx. Next, we sought to test whether the MAF-7 scaffold could perform the biocatalytic cascade for relatively large size substrates. We embedded two other bienzymic systems, urate oxidase (UOx)-dHemin-G4 and xanthine oxidase (XOD)-dHemin-G4, into MAF-7 (denoted as dHemin-G4/UOx@MAF-7 and dHemin-G4/XOD@MAF-7, respectively). As seen in Figures S13 and S14, two substrates, including uric acid (ca. 5.0 × 7.0 Å) and xanthine (ca. 5.0 × 6.9 Å), could both activate the biocatalytic cascade reactions, demonstrating the universality of this encapsulation strategy and the extended scope of catalytic substrates.

Interestingly, we also found the efficient biocatalytic cascade was adaptable to a typical luminol-chemiluminescence (CL) system, in which the biohybrids of dHemin-G4/GOx embedded in MOF could catalyze luminol to produce strong blue light (Figure S15). As displayed in Figure 4A, the biocatalytic cascade activity of dHemin-G4/GOx embedded in MAF-7 was also evidently higher than that in ZIF-90 and ZIF-8 in the presence of glucose. We further investigated the influence of dHemin-G4 and GOx on the catalytic properties of dHemin-G4/GOx@MAF-7: the optimal amount was determined to be 5 μM of dHemin-G4 and 0.5 mg mL^{-1} for GOx (Figure S16), respectively. Significantly, the system of Hemin/GOx@MAF-7 showed very low catalytic activity, which may be attributed to the dimerization of hydrophobic hemin in aqueous solution and the fact that hemin was not conducive to encapsulate into hydrophilic MAF-7 coatings. Compared with the catalytic activity of G4/Hemin/GOx@MAF-7, the covalent attachment of hemin to both ends of G4 (dHemin-G4) encapsulated in dHemin-G4/GOx@MAF-7 greatly boosted this biocatalytic cascade activity in the luminol-based CL system (Figure 4B), further confirming the key role of G4 in enhancing the catalytic activity. Then, the CL spectra (Figure 4C) of the luminol showed that the maximum emission wavelength of the developed systems was around 425 nm, indicating the luminophores in the above systems were the electronically excited-state 3-aminophthalate anions (3-APA*).[50] Thus, the excellent biocatalytic role of dHemin-G4/GOx@MAF-7 was again authenticated in the typical luminol-based CL system.

Protection of MAF-7 to dHemin-G4/GOx. Considering that dHemin-G4/GOx still retained catalytic activity when they were encapsulated in MOF, we decided to explore the protective effect of MAF-7 coatings on dHemin-G4 and GOx in harsh environments. Taking room temperature (RT, 25 ± 1 °C) as control conditions, the enzymatic activity for dHemin-G4/GOx and dHemin-G4/GOx@MAF-7 was detected and compared after incubating the catalysts at 50, 70, and 90 °C (Figure 5A). As anticipated, the relative biocatalytic cascade activity of dHemin-G4/GOx@MAF-7 reduced slower than that of free dHemin-G4/GOx with the increase of temperature, which was ascribed that high temperatures inactivated the naked GOx, demonstrating that MAF-7 coating could protect the inside enzymes from high temperatures. Urea, a chaotropic agent, was selected to examine the protective effect of MAF-7 as it can lead to the loss of biological function by unfolding proteins.[49] Figure 5A displayed that free dHemin-G4/GOx and dHemin-G4/GOx@MAF-7 retained 24.6% and 87.4% of their original activity after exposure to urea, again confirming the superior protection of MAF-7 coatings. Then, dHemin-G4/GOx@MAF-7 maintained 91.3% of its original activity, which was much higher than 19.2% for free dHemin-G4/GOx after protease (trypsin) treatment (Figure 5A). This may result from

https://doi.org/10.1021/acsami.2c18473
ACS Appl. Mater. Interfaces 2022, 14, 54598−54606

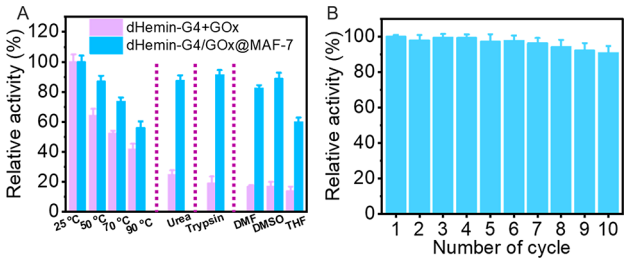

Figure 5. (A) Catalytic activity of dHemin-G4/GOx and dHemin-G4/GOx@MAF-7 after exposure to elevated temperature, urea, trypsin (5 mg mL^{-1}), and organic solvents (DMSO, DMF, and THF) for 4 h. (B) Relative activity of dHemin-G4/GOx@MAF-7 during the cycles. All error bars correspond to the standard deviation (SD) (n = 3).

the size (5.1 × 4.3 × 2.8 nm^3) of trypsin is larger than the pore diameter (ca. 8.6 Å) of MAF-7 and cannot contact the encapsulated enzymes. Finally, we verified the embedded dHemin-G4/GOx was protected by MAF-7 coatings in organic solvents (Figure 5A). Specifically, dHemin-G4/GOx@MAF-7 maintained 82.4%, 87.7%, and 58.8% of its original activity after exposure to DMF, DMSO, and THF, respectively, which was ascribed that the hydrophilic cavity in MAF-7 was not conducive to the entry of organic solvents. In contrast, the activities of free dHemin-G4/GOx were dramatically decreased upon exposure to the same solvents (Figure 5A). These experiments demonstrated that MAF-7 coatings improved the stability of enzymes by providing excellent protection to embedded dHemin-G4/GOx and maintained its catalytic activity in inhospitable environments.

Given the excellent stability of dHemin-G4/GOx@MAF-7, we further cycled dHemin-G4/GOx@MAF-7 10 times and its relative catalytic activity was also retained above 90% (Figure 5B). Furthermore, PXRD analysis and SEM image suggested that the crystallinity and morphology of dHemin-G4/GOx@MAF-7 were maintained after cycling 10 times (Figure S17). Thus, the dHemin-G4/GOx@MAF-7 cascade biosensor was endowed with cost-effective advantage due to such outstanding reusability, which was impossible to supply employing the free cascade biosensor.

Analytical Performance toward Glucose. The practicability of the dHemin-G4/GOx@MAF-7 cascade biosensor for glucose biosensing was also investigated. In this system, the embedded GOx could catalyze glucose to produce H_2O_2, which subsequently oxidized luminol to form luminescent aminophthalic acid in the presence of adjacent dHemin-G4, enabling specific chemiluminescent analysis of glucose (Figure 6A). To improve the sensitivity of the dHemin-G4/GOx@MAF-7 cascade biosensor, we explored the optimal detection conditions of glucose: pH (8.5), 50 μM luminol, and 50 mg L^{-1} catalyst, which were used for subsequent experiments (Figure S18). As expected, the good positive linearity of glucose was 0.01−30 μM with a limit of detection (LOD) of 9.2 nM ($3\delta/K$, in which δ and K indicated the standard deviation of blank samples (n = 11) and slop of the liner regression equation, respectively.) (Figure 6B), which was more sensitive than most reported methods (Table S2). Further, adding a significant excess (from 2- to 300-fold) of some common interfering-molecules (proteins, amino acids, etc.) found in human serum had no effect on the glucose-dHemin/GOx@MAF-7 biocatalytic cascade reaction, indicating good selectivity of the developed biosensor (Figure 6C). Ultimately, the stable, sensitive, and selective dHemin/GOx@MAF-7 cascade biosensor was used for glucose detection of the human serum samples to confirm its potential utility. Importantly, the concentrations of glucose in these samples obtained by the proposed method were well in agreement with those obtained by the glucose GOD-PAP method (Table S3), demonstrating the practicability of the dHemin/GOx@MAF-7 cascade biosensor in complicated samples.

CONCLUSIONS

In conclusion, we developed a simple and efficient encapsulation strategy to confine biocatalytic cascade enzymes in one step using MAF-7 as the scaffold. Compared with the system embedding hemin/GOx in the MAF-7, such MAF-7-confined biocatalytic cascades (dHemin-G4/GOx@MAF-7) present outstanding catalytic activities, which was attributed to dHemin-G4 DNAzyme with high catalytic activity when hemin was covalently linked to both ends of G4. Furthermore, the catalytic activity of MAF-7 confined cascade was significantly higher than the catalytic cascades in the ZIF-8 and ZIF-90, as hydrophilic MAF-7 can increase the embedding content of enzymes. In addition, the versatility of this encapsulation strategy was authenticated on other biocatalytic cascade enzymes in the presence of dHemin-G4 DNAzyme. Moreover, the robust MAF-7-confined microenvironment provided excellent protection to harsh conditions, which endowed the cascade enzymes with high stability and reusability. Our dHemin-G4/GOx@MAF-7 systems have great potentials to mimic biocatalytic cascades happening in cellular environments and are expected to be used in biosensing and industrial fields.

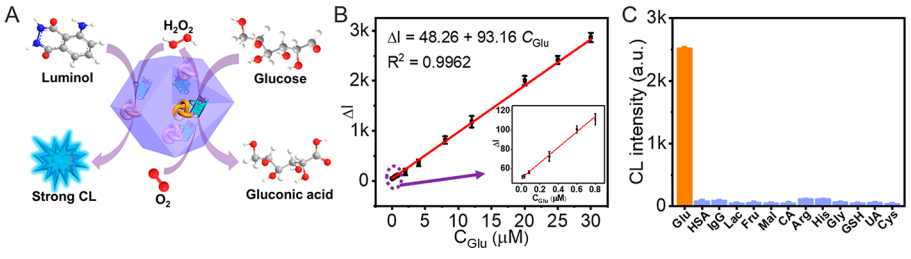

Figure 6. (A) Schematic illustration of the biocatalytic cascade process of dHemin-G4/GOx@MAF-7 system for chemiluminescent measurement of glucose. (B) Linear relationship in net CL intensity versus concentration of glucose. (C) Selectivity of dHemin-G4/GOx@MAF-7 system for glucose analysis.

https://doi.org/10.1021/acsami.2c18473
ACS Appl. Mater. Interfaces 2022, 14, 54598−54606

■ ASSOCIATED CONTENT

Supporting Information

The Supporting Information is available free of charge at https://pubs.acs.org/doi/10.1021/acsami.2c18473.

Discussions of experimental details, tables of comparison of the dHemin-G4 and GOx loading amount with different carriers, comparison of the linear range and LODs for the analysis of glucose based on various methods, and measurement results of glucose in human serum samples, and figures of FT-IR spectra of G4, Hemin, and dHemin-G4 DNAzyme, mass spectrum of dHemin-G4 DNAzyme, SEM image of MAF-7, TEM images of MAF-7 and dHemin-G4/GOx@MAF-7, full X-ray photoelectron spectra and high-resolution XPS spectra (Zn 2p) of MAF-7 and dHemin-G4/GOx@MAF-7, thermogravimetric analysis of MAF-7 and dHemin-G4/GOx@MAF-7, differential pore distributions of MAF-7 and dHemin-G4/GOx@MAF-7, absorption spectra of dHemin-G4, GOx, MAF-7, and dHemin-G4/GOx@MAF-7, peroxidase activity of Hemin, G4/Hemin, Hemin-G4, G4-Hemin, and dHemin-G4 within 60 s, biocatalytic cascade activities of different catalysts in the presence of 1 mM glucose during 10 min, standard curves of protein according to BCA method and hemin, chemical transformation of dHemin-G4/UOx@MAF-7 and dHemin-G4/XOD@MAF-7, chemiluminescence photos of luminol catalyzed by different catalysts, effect of different concentration of GOx and dHemin-G4 on the cascade catalytic activity of dHemin-G4/GOx@MAF-7, PXRD pattern and SEM image of dHemin-G4/GOx@MAF-7 materials after reusing 10 times, and effect of pH, luminol concentration, and catalyst concentration on the catalytic performance of dHemin-G4/GOx@MAF-7 (PDF)

■ AUTHOR INFORMATION

Corresponding Author

Jun Zhou − *State Key Laboratory of Analytical Chemistry for Life Science, School of Chemistry and Chemical Engineering, Nanjing University, Nanjing 210023, P.R. China;* orcid.org/0000-0002-6793-3169; Email: jun.zhou@nju.edu.cn; Fax: (86)-25-89683593

Authors

Xuanxiang Mao − *State Key Laboratory of Analytical Chemistry for Life Science, School of Chemistry and Chemical Engineering, Nanjing University, Nanjing 210023, P.R. China*

Dehui Qiu − *State Key Laboratory of Analytical Chemistry for Life Science, School of Chemistry and Chemical Engineering, Nanjing University, Nanjing 210023, P.R. China*

Shijiong Wei − *State Key Laboratory of Analytical Chemistry for Life Science, School of Chemistry and Chemical Engineering, Nanjing University, Nanjing 210023, P.R. China*

Xiaobo Zhang − *State Key Laboratory of Analytical Chemistry for Life Science, School of Chemistry and Chemical Engineering, Nanjing University, Nanjing 210023, P.R. China;* orcid.org/0000-0003-0222-2515

Jianping Lei − *State Key Laboratory of Analytical Chemistry for Life Science, School of Chemistry and Chemical Engineering, Nanjing University, Nanjing 210023, P.R. China;* orcid.org/0000-0002-3594-180X

Jean-Louis Mergny − *State Key Laboratory of Analytical Chemistry for Life Science, School of Chemistry and Chemical Engineering, Nanjing University, Nanjing 210023, P.R. China; Laboratoire d'Optique et Biosciences, Ecole Polytechnique, CNRS, INSERM, Institut Polytechnique de Paris, 91128 Palaiseau cedex, France*

Huangxian Ju − *State Key Laboratory of Analytical Chemistry for Life Science, School of Chemistry and Chemical Engineering, Nanjing University, Nanjing 210023, P.R. China;* orcid.org/0000-0002-6741-5302

Complete contact information is available at: https://pubs.acs.org/10.1021/acsami.2c18473

Author Contributions

The manuscript was written via contributions of all authors. All authors have given approval to the final version of the manuscript.

Notes

The authors declare no competing financial interest.

■ ACKNOWLEDGMENTS

The work was supported partly by the National Natural Science Foundation of China (21977045, 22177047, 22004062, and 22104063), State Key Laboratory of Analytical Chemistry for Life Science (5431ZZXM2202), China Postdoctoral Science Foundation (2021M702106), and the Fundamental Research Funds for the Central Universities (202200324 and 202200325).

■ REFERENCES

(1) Man, T.; Xu, C.; Liu, X. Y.; Li, D.; Tsung, C. K.; Pei, H.; Wan, Y.; Li, L. Hierarchically Encapsulating Enzymes with Multi-Shelled Metal-Organic Frameworks for Tandem Biocatalytic Reactions. *Nat. Commun.* **2022**, *13*, 305−317.

(2) Quin, M. B.; Wallin, K. K.; Zhang, G.; Schmidt-Dannert, C. Spatial Organization of Multi-Enzyme Biocatalytic Cascades. *Org. Biomol. Chem.* **2017**, *15*, 4260−4271.

(3) Chen, W. H.; Vázquez-González, M.; Zoabi, A.; Abu-Reziq, R.; Willner, I. Biocatalytic Cascades Driven by Enzymes Encapsulated in Metal-Organic Framework Nanoparticles. *Nat. Catal.* **2018**, *1*, 689−695.

(4) Good, M. C.; Zalatan, J. G.; Lim, W. A. Scaffold Proteins: Hubs for Controlling the Flow of Cellular Information. *Science* **2011**, *332*, 680−685.

(5) Barabasi, A. L.; Oltvai, Z. N. Network Biology: Understanding the Cell's Functional Organization. *Nat. Rev. Genet.* **2004**, *5*, 101−113.

(6) Zhu, H.; Li, X. L.; He, Z. M.; Chen, Y.; Zhu, J. J. Metal Azolate Coordination Polymer-Enabled High Payload and Non-Destructive Enzyme Immobilization for Biocatalysis and Biosensing. *Anal. Chem.* **2022**, *94*, 6827−6832.

(7) Liu, X.; Qi, W.; Wang, Y.; Su, R.; He, Z. A Facile Strategy for Enzyme Immobilization with Highly Stable Hierarchically Porous Metal-Organic Frameworks. *Nanoscale* **2017**, *9*, 17561−17570.

(8) Vázquez-González, M.; Wang, C.; Willner, I. Biocatalytic Cascades Operating on Macromolecular Scaffolds and in Confined Environments. *Nat. Catal.* **2020**, *3*, 256−273.

(9) Tang, Z.; Li, X.; Tong, L.; Yang, H.; Wu, J.; Zhang, X.; Song, T.; Huang, S.; Zhu, F.; Chen, G. S.; Ouyang, G. F. A Biocatalytic Cascade in an Ultrastable Mesoporous Hydrogen-Bonded Organic Framework for Point-of-Care Biosensing. *Angew. Chem., Int. Ed.* **2021**, *60*, 23608−23613.

(10) Chiang, C. W.; Liu, X.; Sun, J.; Guo, J.; Tao, L.; Gao, W. Polymerization-Induced Coassembly of Enzyme-Polymer Conjugates into Comicelles with Tunable and Enhanced Cascade Activity. *Nano Lett.* **2020**, *20*, 1383−1387.
(11) Lu, S.; Hu, T.; Wang, S.; Sun, J.; Yang, X. Ultra-Sensitive Colorimetric Assay System Based on the Hybridization Chain Reaction-Triggered Enzyme Cascade Amplification. *ACS Appl. Mater. Interfaces* **2017**, *9*, 167−175.
(12) Liao, C. A.; Wu, Q.; Wei, Q. C.; Wang, Q. G. Bioinorganic Nanocomposite Hydrogels Formed by HRP-GOx-Cascade-Catalyzed Polymerization and Exfoliation of the Layered Composites. *Chem. Eur. J.* **2015**, *21*, 12620−12626.
(13) Zhang, Y.; Yong, Y.; Ge, J.; Liu, Z. Lectin Agglutinated Multienzyme Catalyst with Enhanced Substrate Affinity and Activity. *ACS Catal.* **2016**, *6*, 3789−3795.
(14) Zore, O. V.; Pattammattel, A.; Gnanaguru, S.; Kumar, C. V.; Kasi, R. M. Bienzyme-Polymer-Graphene Oxide Quaternary Hybrid Biocatalysts: Efficient Substrate Channeling under Chemically and Thermally Denaturing Conditions. *ACS Catal.* **2015**, *5*, 4979−4988.
(15) Zhang, L.; Fan, C.; Liu, M.; Liu, F.; Bian, S.; Du, S.; Zhu, S.; Wang, H. Biominerized Gold-Hemin@MOF Composites with Peroxidase-like and Gold Catalysis Activities: A High-Throughput Colorimetric Immunoassay for Alpha-Fetoprotein in Blood by Elisa and Gold-Catalytic Silver Staining. *Sens. Actuators, B* **2018**, *266*, 543−552.
(16) Wu, J.; Wang, X.; Wang, Q.; Lou, Z.; Li, S.; Zhu, Y.; Qin, L.; Wei, H. Nanomaterials with Enzyme-Like Characteristics (Nanozymes): Next-Generation Artificial Enzymes (II). *Chem. Soc. Rev.* **2019**, *48*, 1004−1076.
(17) Mergny, J. L.; Sen, D. DNA Quadruple Helices in Nanotechnology. *Chem. Rev.* **2019**, *119*, 6290−6325.
(18) Alsharabasy, A. M.; Pandit, A.; Farras, P. Recent Advances in the Design and Sensing Applications of Hemin/Coordination Polymer-Based Nanocomposites. *Adv. Mater.* **2021**, *33*, 2003883.
(19) Guo, Y. J.; Deng, L.; Li, J.; Guo, S. J.; Wang, E. K.; Dong, S. J. Hemin-Graphene Hybrid Nanosheets with Intrinsic Peroxidase-Like Activity for Label-Free Colorimetric Detection of Single-Nucleotide Polymorphism. *ACS Nano* **2011**, *5*, 1282−1290.
(20) Luo, F.; Lin, Y.; Zheng, L.; Lin, X.; Chi, Y. Encapsulation of Hemin in Metal-Organic Frameworks for Catalyzing the Chemiluminescence Reaction of the H_2O_2-Luminol System and Detecting Glucose in the Neutral Condition. *ACS Appl. Mater. Interfaces* **2015**, *7*, 11322−11329.
(21) Zhu, N.; Liu, C.; Liu, R.; Niu, X.; Xiong, D.; Wang, K.; Yin, D.; Zhang, Z. Biomimic Nanozymes with Tunable Peroxidase-Like Activity Based on the Confinement Effect of Metal-Organic Frameworks (MOFs) for Biosensing. *Anal. Chem.* **2022**, *94*, 4821−4830.
(22) Mao, X. X.; He, F. N.; Qiu, D. H.; Wei, S. J.; Luo, R. G.; Chen, Y.; Zhang, X. B.; Lei, J. P.; Monchaud, D.; Mergny, J. L.; Ju, H. X.; Zhou, J. Efficient Biocatalytic System for Biosensing by Combining Metal-Organic Framework (MOF)-Based Nanozymes and G-Quadruplex (G4)-DNAzymes. *Anal. Chem.* **2022**, *94*, 7295−7302.
(23) Chen, Y.; Qiu, D.; Zhang, X.; Liu, Y.; Cheng, M.; Lei, J.; Mergny, J. L.; Ju, H.; Zhou, J. Highly Sensitive Biosensing Applications of a Magnetically Immobilizable Covalent G-Quadruplex-Hemin DNAzyme Catalytic System. *Anal. Chem.* **2022**, *94*, 2212−2219.
(24) Wang, Z. G.; Wang, H.; Liu, Q.; Duan, F.; Shi, X.; Ding, B. Designed Self-Assembly of Peptides with G-Quadruplex/Hemin DNAzyme into Nanofibrils Possessing Enzyme-Mimicking Active Sites and Catalytic Functions. *ACS Catal.* **2018**, *8*, 7016−7024.
(25) Travascio, P.; Li, Y. F.; Sen, D. DNA-Enhanced Peroxidase Activity of a DNA Aptamer-Hemin Complex. *Chem. Biol.* **1998**, *5*, 505−517.
(26) Sen, D.; Poon, L. C. RNA and DNA Complexes with Hemin [Fe(III) Heme] Are Efficient Peroxidases and Peroxygenases: How Do They Do It and What Does It Mean? *Crit. Rev. Biochem. Mol. Biol.* **2011**, *46*, 478−492.
(27) Yum, J. H.; Park, S.; Sugiyama, H. G-Quadruplexes as Versatile Scaffolds for Catalysis. *Org. Biomol. Chem.* **2019**, *17*, 9547−9561.
(28) Li, W.; Li, Y.; Liu, Z.; Lin, B.; Yi, H.; Xu, F.; Nie, Z.; Yao, S. Insight into G-Quadruplex-Hemin DNAzyme/RNAzyme: Adjacent Adenine as the Intramolecular Species for Remarkable Enhancement of Enzymatic Activity. *Nucleic Acids Res.* **2016**, *44*, 7373−7384.
(29) Canale, T. D.; Sen, D. Hemin-Utilizing G-Quadruplex DNAzymes are Strongly Active in Organic Co-Solvents. *Biochim. Biophys. Acta* **2017**, *1861*, 1455−1462.
(30) Chen, J.; Guo, Y.; Zhou, J.; Ju, H. The Effect of Adenine Repeats on G-quadruplex/hemin Peroxidase Mimicking DNAzyme Activity. *Chem. Eur. J.* **2017**, *23*, 4210−4215.
(31) Chen, J.; Zhang, Y.; Cheng, M.; Mergny, J. L.; Lin, Q.; Zhou, J.; Ju, H. Highly Active G-quadruplex/hemin DNAzyme for Sensitive Colorimetric Determination of Lead(II). *Microchim. Acta* **2019**, *186*, 786.
(32) Qiu, B.; Zheng, Z. Z.; Lu, Y. J.; Lin, Z. Y.; Wong, K. Y.; Chen, G. N. G-Quadruplex DNAzyme as the Turn on Switch for Fluorimetric Detection of Genetically Modified Organisms. *Chem. Commun.* **2011**, *47*, 1437−1439.
(33) Gao, Y.; Li, B. Exonuclease III-Assisted Cascade Signal Amplification Strategy for Label-Free and Ultrasensitive Chemiluminescence Detection of DNA. *Anal. Chem.* **2014**, *86*, 8881−8887.
(34) Luo, M.; Chen, X.; Zhou, G.; Xiang, X.; Chen, L.; Ji, X.; He, Z. Chemiluminescence Biosensors for DNA Detection Using Graphene Oxide and a Horseradish Peroxidase-Mimicking DNAzyme. *Chem. Commun.* **2012**, *48*, 1126−1128.
(35) Shen, P.; Li, W.; Liu, Y.; Ding, Z.; Deng, Y.; Zhu, X.; Jin, Y.; Li, Y.; Li, J.; Zheng, T. High-Throughput Low-Background G-Quadruplex Aptamer Chemiluminescence Assay for Ochratoxin a Using a Single Photonic Crystal Microsphere. *Anal. Chem.* **2017**, *89*, 11862−11868.
(36) Zhu, L.; Li, C.; Zhu, Z.; Liu, D.; Zou, Y.; Wang, C.; Fu, H.; Yang, C. In Vitro Selection of Highly Efficient G-Quadruplex-Based DNAzymes. *Anal. Chem.* **2012**, *84*, 8383−8390.
(37) Stefan, L.; Xu, H. J.; Gros, C. P.; Denat, F.; Monchaud, D. Harnessing Nature's Insights: Synthetic Small Molecules with Peroxidase-Mimicking DNAzyme Properties. *Chem. Eur. J.* **2011**, *17*, 10857−10862.
(38) Liang, W.; Xu, H.; Carraro, F.; Maddigan, N. K.; Li, Q.; Bell, S. G.; Huang, D. M.; Tarzia, A.; Solomon, M. B.; Amenitsch, H.; Vaccari, L.; Sumby, C. J.; Falcaro, P.; Doonan, C. J. Enhanced Activity of Enzymes Encapsulated in Hydrophilic Metal-Organic Frameworks. *J. Am. Chem. Soc.* **2019**, *141*, 2348−2355.
(39) Liang, W.; Wied, P.; Carraro, F.; Sumby, C. J.; Nidetzky, B.; Tsung, C. K.; Falcaro, P.; Doonan, C. J. Metal-Organic Framework-Based Enzyme Biocomposites. *Chem. Rev.* **2021**, *121*, 1077−1129.
(40) Liang, J.; Liang, K. Multi-Enzyme Cascade Reactions in Metal-Organic Frameworks. *Chem. Rec.* **2020**, *20*, 1100−1116.
(41) Sheng, T. R.; Guan, X.; Liu, C.; Su, Y. D. De Novo Approach to Encapsulating Biocatalysts into Synthetic Matrixes: From Enzymes to Microbial Electrocatalysts. *ACS Appl. Mater. Interfaces* **2021**, *13*, 52234−52249.
(42) Chen, G.; Kou, X.; Huang, S.; Tong, L.; Shen, Y.; Zhu, W.; Zhu, F.; Ouyang, G. Modulating the Biofunctionality of Metal-Organic-Framework-Encapsulated Enzymes through Controllable Embedding Patterns. *Angew. Chem., Int. Ed.* **2020**, *59*, 2867−2874.
(43) Liao, F. S.; Lo, W. S.; Hsu, Y. S.; Wu, C. C.; Wang, S. C.; Shieh, F. K.; Morabito, J. V.; Chou, L. Y.; Wu, K. C.; Tsung, C. K. Shielding against Unfolding by Embedding Enzymes in Metal-Organic Frameworks Via a De Novo Approach. *J. Am. Chem. Soc.* **2017**, *139*, 6530−6533.
(44) Ricco, R.; Liang, W.; Li, S.; Gassensmith, J. J.; Caruso, F.; Doonan, C.; Falcaro, P. Metal-Organic Frameworks for Cell and Virus Biology: A Perspective. *ACS Nano* **2018**, *12*, 13−23.
(45) Doonan, C.; Ricco, R.; Liang, K.; Bradshaw, D.; Falcaro, P. Metal-Organic Frameworks at the Biointerface: Synthetic Strategies and Applications. *Acc. Chem. Res.* **2017**, *50*, 1423−1432.

https://doi.org/10.1021/acsami.2c18473
ACS Appl. Mater. Interfaces 2022, 14, 54598−54606

(46) Zoungrana, T.; Findenegg, G. H.; Norde, W. Structure, Stability, and Activity of Adsorbed Enzymes. *J. Colloid Interface Sci.* **1997**, *190*, 437−448.
(47) Khaldi, K.; Sam, S.; Lounas, A.; Yaddaden, C.; Gabouze, N. E. Comparative Investigation of Two Methods for Acetylcholinesterase Enzyme Immobilization on Modified Porous Silicon. *Appl. Surf. Sci.* **2017**, *421*, 148−154.
(48) Wang, Q. B.; Xu, N.; Gui, Z.; Lei, J. P.; Ju, H. X.; Yan, F. Catalytic Activity of a Dual-Hemin Labelled Oligonucleotide: Conformational Dependence and Fluorescent DNA Sensing. *Chem. Commun.* **2014**, *50*, 15362−15365.
(49) Monera, O. D.; Kay, C. M.; Hodges, R. S. Protein Denaturation with Guanidine Hydrochloride or Urea Provides a Different Estimate of Stability Depending on the Contributions of Electrostatic Interactions. *Protein Sci.* **1994**, *3*, 1984−1991.
(50) Mao, X. X.; Lu, Y. W.; Zhang, X. D.; Huang, Y. M. *β*-Cyclodextrin Functionalization of Metal-Organic Framework MOF-235 with Excellent Chemiluminescence Activity for Sensitive Glucose Biosensing. *Talanta* **2018**, *188*, 161−167.

https://doi.org/10.1021/acsami.2c18473
ACS Appl. Mater. Interfaces 2022, 14, 54598−54606